

Characterization of nonlinear spectral linewidth and light shift in diffuse laser-cooled atoms

Yiran Yin(殷怡然), An-Ning Xu(许安宁), Jin Peng(彭瑾), and Bei Liu(刘贝)

Citation : Chin. Phys. B, 2025, 34 (**2**): 023401. DOI: 10.1088/1674-1056/ad990f
Journal homepage: http://cpb.iphy.ac.cn; http://iopscience.iop.org/cpb

What follows is a list of articles you may be interested in

Interaction of H_2^+ molecular beam with thin layer graphene foils

Min Li(李敏), Guo-Feng Qu(曲国峰), Yi-Zhou Wang(王亦舟), Zhou-Sen Zhu(朱洲森), Mian-Gong Shi(师勉恭), Mao-Lei Zhou(周茂蕾), Dong Liu(刘东), Zi-Xu Xu(徐子虚), Ming-Jiang Song(宋明江), Jun Zhang(张俊), Fan Bai(白帆), Xiao-Dong Liao(廖小东), Ji-Feng Han(韩纪锋)
Chin. Phys. B, 2019, 28 (**9**): 093401. DOI: 10.1088/1674-1056/ab33f2

Landau-Zener model for electron loss of low-energy negative fluorine ions to surface cations during grazing scattering on a LiF (001) surface

Wang Zhou(周旺), Meixiao Zhang(张鹂枭), Lihua Zhou(周利华), Hu Zhou(周虎), Yulong Ma(马玉龙), Yanling Guo(郭艳玲), Lin Chen(陈林), Ximeng Chen(陈熙萌)
Chin. Phys. B, 2016, 25 (**11**): 113401. DOI: 10.1088/1674-1056/25/11/113401

Understanding charge transfer of Li^+ and Na^+ ions scattered from metal surfaces with high work function

Lin Chen(陈林), Wen-Bin Wu(武文斌), Pin-Yang Liu(刘品阳), Yun-Qing Xiao(肖云青), Guo-Peng Li(李国朋), Yi-Ran Liu(刘亦然), Hao-Yu Jiang(江浩雨), Yan-Ling Guo(郭艳玲), Xi-Meng Chen(陈熙萌)
Chin. Phys. B, 2016, 25 (**8**): 083401. DOI: 10.1088/1674-1056/25/8/083401

Photodetachment microscopy of H^- in the magnetic field near different dielectric surfaces

Tang Tian-Tian (唐田田), Zhang Min (张敏), Zhang Chao-Min (张朝民)
Chin. Phys. B, 2015, 24 (**6**): 063401. DOI: 10.1088/1674-1056/24/6/063401

Control of the photodetachment of H^- near a metallic sphere surface by an elastic interface

Li Shao-Sheng (李绍晟), Wang De-Hua (王德华)
Chin. Phys. B, 2014, 23 (**2**): 023402. DOI: 10.1088/1674-1056/23/2/023402

Characterization of nonlinear spectral linewidth and light shift in diffuse laser-cooled atoms

Yiran Yin(殷怡然), An-Ning Xu(许安宁), Jin Peng(彭瑾), and Bei Liu(刘贝)†

Key Laboratory of Laser and Infrared System, Ministry of Education, Center for Optics Research and Engineering (CORE), Shandong University, Qingdao 266237, China

(Received 12 September 2024; revised manuscript received 14 November 2024; accepted manuscript online 2 December 2024)

We demonstrate an integrating sphere to cool ^{87}Rb atoms and measure the recoil-induced resonance and electromagnetically induced absorption spectrum. We measure the relationship between their linewidth and light shift with variation of the detuning and power of the cooling laser and study the performance of the diffuse laser cooling mechanism by the absorption linewidth radio $\Delta\nu_{\rm E}/\Delta\nu_{\rm R}$ and light shift $|\Delta_{\rm R}-\Delta_{\rm E}|$ using nonlinear spectroscopy. Specifically, when $\Delta\nu_{\rm E}/\Delta\nu_{\rm R}$ reaches a value of 1.57, the temperature and number of cold atoms achieve the optimal cooling effect. This characterization of absorption linewidth and light shift will provide a method to estimate whether diffuse light cooling achieves the best cooling effect, contributing to the future development of isotropic laser cooling for application in quantum sensing.

Keywords: nonlinear spectrum, diffuse laser cooling, temperature measurement

PACS: 34.35.+a, 37.10.De, 47.80.Cb, 82.53.Kp

DOI: 10.1088/1674-1056/ad990f **CSTR:** 32038.14.CPB.ad990f

1. Introduction

Cold atom magnetometers have been widely applied to measurement of weak magnetic fields, including magnetic induction imaging,[1–3] magnetic resonance in a vector field,[4–7] and vacuum-related applications.[8–11] Magneto-optical traps (MOTs)[12,13] have served as the primary cooling apparatus for achieving cold atomic magnetometers. However, a special arrangement of laser beams and a quadrupole magnetic field are needed, which results in atomic perturbation by the nonzero magnetic field and may exert an influence on the measuring performance. In contrast, laser cooling of atoms in diffuse light has shown great potential in many applications and is a good candidate for building an atomic magnetometer due to the compact setup and simpler structure without external magnetic fields. The sensitivity of the magnetometer is critically dependent on the relaxation time and number of cold atoms;[14] the relaxation time relies on the atomic temperature, therefore identifying the appropriate measuring method for calibrating the atomic temperature and number remains a major research concern. A nonlinear spectroscopy technique for estimating the temperature and number of confined cold atoms can be an effective instrument for studying physical processes in an integrating sphere cold atom magnetometer. Consequently, we propose to explore the physical mechanism using the nonlinear spectrum to extract information about cold atoms in the integrating sphere, such as atomic temperature and atomic density.

Current research on the nonlinear spectroscopy of cold atoms mainly focuses on stimulated Raman scattering,[15,16] recoil-induced resonances (RIR),[17,18] electromagnetic-induced transparency[19,20] and electromagnetically induced absorption (EIA).[21,22] Traditional cooling mechanisms, such as MOTs [23] and optical lattices,[24,25] have typically measured the RIR or EIA signals. The coexisting nonlinear spectroscopy of cold atoms has been observed in the integrating sphere cooling scheme.[26] Within the integrating sphere, RIR has the potential for non-destructive temperature measurement, [27] while the light shift of EIA is used to extract the effective Rabi frequency.[28] The latter research focused on the individual roles of RIR and EIA signals in a diffuse light field. In this work, we focus on the relationship between two signals in the integrating sphere with changes in the cooling power and detuning. Since the RIR and EIA signals exist simultaneously in the integrating sphere cooling scheme, diffuse light has a different effect on each signal. By exploring the relationship between the two signals, including their linewidth ratio and light shift, we further explore the optimal cooling conditions and underlying mechanisms within a diffuse light field.

In this paper, we obtain the temperature and number of cold atoms by measuring both RIR and EIA nonlinear spectra in the integrating sphere. Firstly, we analyze the physical characterization of the RIR and EIA nonlinear spectra. Then, we measure the different nonlinear spectral signals by varying the detuning and power of the cooling laser. Utilizing the distinct characteristics of the two absorption resonances, we define the absorption linewidths of the RIR and EIA as $\Delta\nu_{\rm R}$ and $\Delta\nu_{\rm E}$, respectively. The values of the probe laser detuning that

†Corresponding author. E-mail: beiliu@sdu.edu.cn

© 2025 Chinese Physical Society and IOP Publishing Ltd. All rights, including for text and data mining, AI training, and similar technologies, are reserved.

correspond to the RIR and EIA peaks are $\Delta_{\rm R}$ and $\Delta_{\rm E}$, respectively. We can directly extract the difference value $|\Delta_{\rm R}-\Delta_{\rm E}|$ of the light shift and the ratio $\Delta\nu_{\rm E}/\Delta\nu_{\rm R}$ of their absorption linewidths with cooling laser power and detuning. Subsequently, $\Delta\nu_{\rm E}/\Delta\nu_{\rm R}$ allows us to ascertain the optimal cooling conditions for determining the temperature and number of cold atoms. Furthermore, we explore the contribution of the diffuse light field to the coexistence of both signals and compare the temperature measurement result between the RIR width and the time-of-flight (TOF) method. Our work will help provide a novel approach for the quantitative assessment of cold atom temperature and number, thereby establishing a foundation for the subsequent study of cold atom magnetometers in a diffuse light field.

2. Physical characterization of RIR and EIA spectra

A simple description of the physical characterization underlying RIR is as follows. The cooling laser is used as the pump laser, with the wave vector, frequency, Rabi frequency and detuning frequency denoted by $k_{\rm c}$, $\omega_{\rm c}$, $\Omega_{\rm c}$ and $\Delta_{\rm c}$ ($\Delta_{\rm c}=\omega_{\rm c}-\omega_0$, ω_0 is the resonance frequency of atomic transition), respectively. The probe laser has a wave vector $k_{\rm p}$, frequency $\omega_{\rm p}$, Rabi frequency $\Omega_{\rm p}$ and detuning frequency $\Delta_{\rm p}=\omega_{\rm p}-\omega_0$. The detuning between the probe laser and cooling laser is defined by $\Delta=\omega_{\rm p}-\omega_{\rm c}$. The angle between the cooling and probe lasers is θ. Assuming that the probe-cooling detuning Δ is sufficiently small, one can find that $|k_{\rm p}|\approx|k_{\rm c}|=k$. The RIR appears on the transmission spectrum of the probe laser, and can be interpreted as a stimulated Raman process between two different momentum states. Indeed, due to this stimulated Raman process, when $\Delta>0$, the probe signal is absorbed, when $\Delta<0$, the probe signal is amplified. The RIR structure shows a dispersion-like shape. The process of cooling photon absorption followed by probe photon emission results in momentum change of the atoms: the calculation of the angle θ is related to the momentum p,[23,29]

$$|\Delta|=\frac{2k}{m}(\hbar k\sin\frac{\theta}{2}-p)\sin\frac{\theta}{2}. \tag{1}$$

Now we consider the particularity of diffuse light-decelerating atoms in the integrating sphere. Given that the cooling laser in the integrating sphere is effectively diffuse light after multiple reflections,[26] an atom with velocity ν resonates with the photons whose propagating directions are at an angle α with ν. The cooling laser detuning must satisfy $\Delta_{\rm c}-k_{\rm c}\nu\cos\alpha=0$ to automatically compensate for the Doppler shift. The cooling laser entering the integrating sphere through the multimode fiber does not undergo diffuse reflection before it touches the inner surface of the integrating sphere, and it forms four extended lasers perpendicular to the direction of the probe laser. The angle between these extended lasers and the probe laser is close to $\pi/2$ rad, which is too large to generate the RIR two-photon process. Consequently, only when the angle θ is sufficiently small, the RIR signal is produced. Unlike θ in the MOT is easy to manipulate, the diffuse light field generated by the cooling laser entering the integrating sphere is complex, and θ is constantly changing. We need to find a critical angle $\theta_{\rm c}$ such that the range of $0<\theta<\theta_{\rm c}$ can show RIR with the majority of cold atoms. $\theta_{\rm c}$ can be calculated using the law of conservation of energy, where the momentum changes of the two-photon process need to match the energy change of the diffuse light in the integrating sphere[26,27]

$$\begin{aligned}4\pi m(\omega_{\rm p}-\omega_{\rm c}) &= 2k_{\rm p}p_x+2k_{\rm c}(p_x\cos\theta_{\rm c}-p_y\sin\theta_{\rm c})\\ &\quad+\hbar(k_{\rm p}^2+k_{\rm c}^2+2k_{\rm p}k_{\rm c}\cos\theta_{\rm c}).\end{aligned} \tag{2}$$

For an atom with initial momentum p_x in the direction $\boldsymbol{e}_x$ and momentum p_y in the direction $\boldsymbol{e}_y$, p_x and p_y are all positive. By considering the simplification in Ref. [26], $\theta_{\rm c}$ is approximately 0.122 rad in our best experimental conditions. The RIR gain is proportional to the population difference of two momentum states[29]

$$G_{\rm RIR}=-2\pi N_0\frac{\Omega_{\rm p}^*|\Omega_{\rm c}|^2\omega_k p^2}{\Delta_{\rm c}^2k^2\nu^2}W'\left(-\frac{p|\Delta|}{2k\nu}\right), \tag{3}$$

where N_0 is the atomic number, ν is the atomic velocity, $W(p)=\mathrm{e}^{-p^2/p_0^2}/(\sqrt{\pi}p_0)^3$ is the one-dimensional momentum distribution function, p_0 is the atomic initial momentum and W' is its first-order derivative with respect to p, $\omega_k=\hbar k^2/2m$ is the recoil frequency and m is the atomic mass. The RIR gain is a dispersion-like line shape centered around $\Delta=0$, the distance between the peaks of which (RIR width)[30,31] is $\Delta W_{\rm RIR}=2k\theta_{\rm c}\sqrt{k_{\rm B}T/m}$.

The EIA arises from the transfer of coherence from the excited state Zeeman sublevels to the ground state Zeeman sublevels, facilitated by the spontaneous emission process induced by the coupled light fields. This coherence manifests as constructive interference, where the Zeeman sublevels within the same ground state are coupled together and mutually reinforce each other through spontaneous emission. The EIA involves constructive interference across multiple quantum pathways participating in the transition, leading to an increased population of atoms in a particular quantum state and consequently enhancing probe absorption. The EIA model is obtained by summing the Lorentzian profiles centered at the appropriate resonance frequencies and weighted by the products of the relevant population differences and the square of the Clebsch–Gordan coefficients as[30]

$$\begin{aligned}G_{\rm EIA}(\delta) &= \sum_{i=1}^{2}w_{i-1,i}\Delta\Pi_{i-1,i}L(\delta,\delta_{i-1,i},\gamma_{i-1,i})\\ &\quad-\sum_{i=-1}^{-2}w_{i+1,i}\Delta\Pi_{i+1,i}L(\delta,\delta_{i+1,i},\gamma_{i+1,i}),\end{aligned} \tag{4}$$

where $w_{k,j}$ is the weight associated with the Clebsch–Gordan coefficient along the $k = m_g \longleftrightarrow j = m_g$ Raman transition path, $\Delta\Pi_{k,j}$ is the population difference of the $k = m_g$ and $j = m_g$ sublevels and the Lorentzian profile is given by $L(\delta, \delta_{k,j}, \gamma_{k,j}) = \frac{\gamma_{k,j}}{\gamma_{k,j}^2 + (\delta - \delta_{k,j})^2}$, where $\delta_{k,j}$ represents the resonance frequencies and $\gamma_{k,j}$ represents the widths of the $k = m_g \longleftrightarrow j = m_g$ transitions. The primary reason for the light shift in EIA is the interaction between the Zeeman sublevels in the ground state of cold atoms. The EIA peak signal at the energy position corresponds to the light shift between adjacent sublevels, and its amplitude is proportional to the product of the relevant population differences and the Clebsch–Gordan coefficients involved in the specific transition.

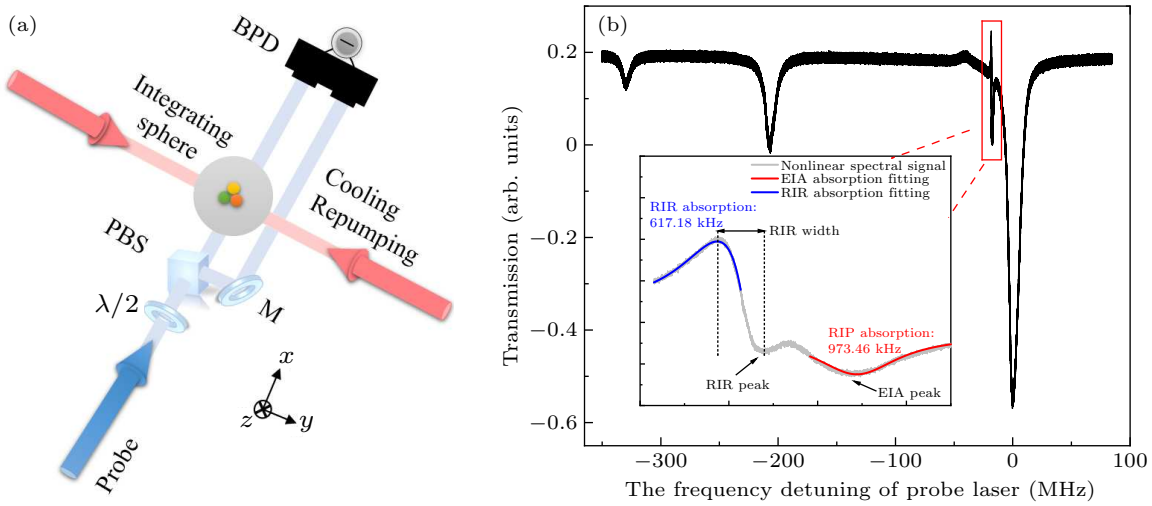


Fig. 1. (a) Schematic diagram of differential detection (PBS, polarized beam splitter; BPD, balanced photodetector; M, mirror). The combined cooling and repumping laser is separated into four parts and injected into the integrating sphere, while the probe laser is perpendicular to them. Differential detection can effectively suppress the common-mode noise and improve the signal-to-noise ratio. (b) The hyperfine structure absorption spectrum is recorded by scanning the frequency of the probe laser across the transition $|5^2S_{1/2}, F = 2\rangle \rightarrow |5^2P_{3/2}, F' = 1, 2, 3\rangle$. The red square is the nonlinear spectrum signal, which can be superimposed by the RIR and EIA. Inset: under the condition that the cooling laser power and detuning are about 320 mW and -19 MHz, the blue and red lines represent the Lorentzian fitting curves of the RIR and EIA absorption peak spectra, with linewidths of 617.18 kHz and 973.46 kHz, respectively. The RIR width, the RIR peak and the EIA peak are indicated with black arrows to facilitate subsequent study in the nonlinear spectrum.

3. Experimental setup

We utilize an integrating sphere to generate isotropic diffuse light for the direct laser cooling of atoms. A cylindrical glass cell, with an inner diameter of 47 mm and a length of 100 mm, is mounted on an ion pump and linked to a rubidium reservoir. This setup maintains a background pressure of 10^{-9} Torr. The glass cell is enveloped by an integrating sphere crafted from polytetrafluoroethylene, which exhibits a diffuse reflection coefficient at the inner surface of 98% at 780 nm.

In our experiment, the cooling laser, with a total power of 320 mW, is red-detuned about 19 MHz ($\sim 3\Gamma$) to the $|5^2S_{1/2}, F = 2\rangle \rightarrow |5^2P_{3/2}, F' = 3\rangle$ transition. The repumping laser is locked to the $|5^2S_{1/2}, F = 1\rangle \rightarrow |5^2P_{3/2}, F' = 2\rangle$ transition with a power of 10 mW, used to keep the population from being trapped in the $|5^2S_{1/2}, F = 2\rangle$ state. The combined cooling and repumping lasers are delivered through two pairs of vertically mounted multimode fibers positioned in the central plane of the integrating sphere.

As shown in Fig. 1(a), the probe laser, with a power of 1.5 μW, is split equally by a polarized beam splitter. One is directly reflected in free space using a mirror, while the other is transmitted horizontally through the cold atoms. Finally, the differential signal of the probe laser is measured by a balanced photodetector. By sweeping the frequency of the probe laser among the atomic resonance, we measure the atomic absorption spectrum as shown in Fig. 1(b). The reduction of the Doppler width of the cold atoms allows resolution of the atomic hyperfine structure. The weak amplification and absorption signals near the absorption peak constitute the nonlinear spectrum signal, as depicted in the red square in Fig. 1(b), which can be decomposed into the RIR and EIA signals.

4. Experimental results and discussion

We first measure the different nonlinear spectral signals by varying the detuning and power of the cooling laser to obtain the RIR width. As shown in Figs. 2(a) and 2(b), the sweep frequency range of the probe laser is approximately 15 MHz and its power is about 1 μW. It is observed that the nonlinear spectral signal associated with the cold atoms consistently appears near the frequency at which the detuning of the probe laser matches that of the cooling laser. The frequency position of the RIR signal remains invariant with changes in the power of the cooling laser, which is a notable characteristic distinguishing the RIR signal from the stimulated Raman scattering signal observed in cold atoms.

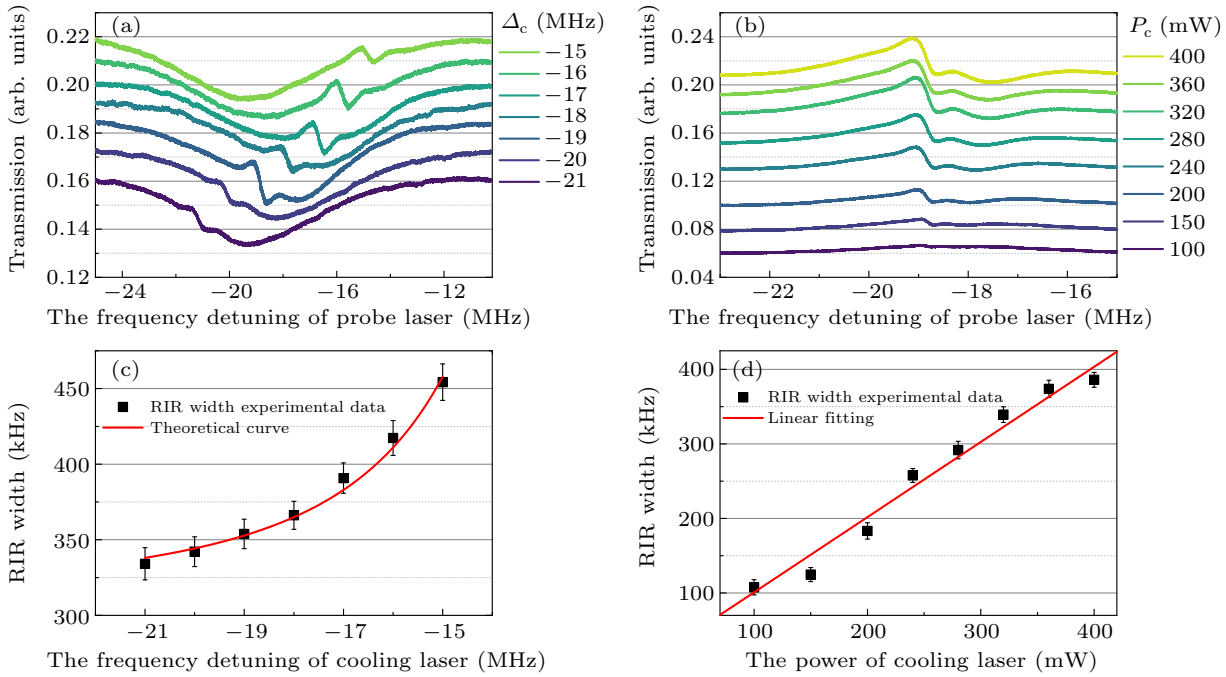


Fig. 2. [(a) and (b)] Experimental signal of the nonlinear spectra of cold atoms varying with the detuning Δ_c and power P_c of the cooling laser. The sweep range and power of the probe laser are about 15 MHz and 1 μW, respectively. (c) The black squares represent the experimental data for RIR width and the red line is the theoretical curve for RIR width with increase in detuning of the the cooling laser. (d) The black squares represent the experimental data for RIR width and the red line is the linear fitting of RIR width with increase in cooling laser power. The RIR width shows power broadening with increase in the cooling laser power.

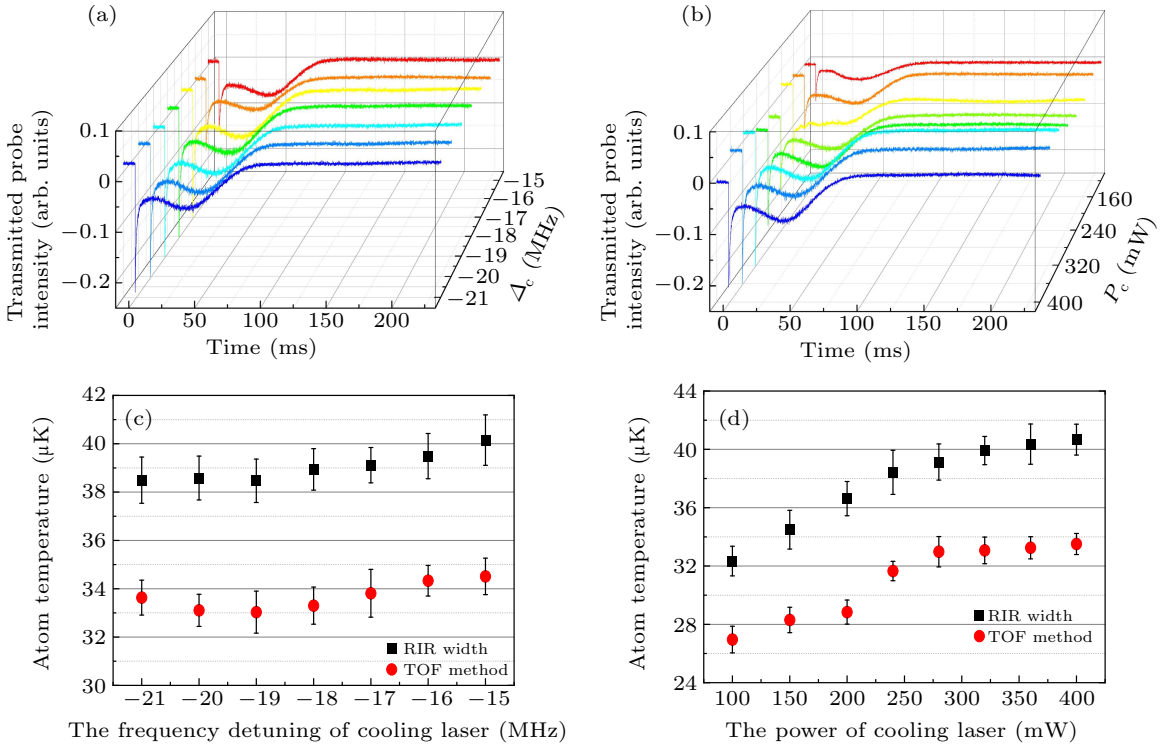


Fig. 3. [(a) and (b)] TOF signal at different detunings and powers of the cooling laser. [(c) and (d)] The temperature of cold atoms measured by the TOF method and RIR width compared under different cooling laser detunings and powers. The black squares and red circles represent the atomic temperature obtained from the RIR width and TOF method, respectively.

We calculate the RIR width (the distance between two peaks) for different detunings and powers of the cooling laser. As the detuning of the cooling laser increases, the RIR width gradually narrows. This occurs because the RIR induces changes in the ground state population of cold atoms across different velocity distributions and the relationship between the RIR width and the lasering of the cooling laser Δ_c, as shown by $\Delta W_{\mathrm{RIR}} = \frac{2\hbar k^3\theta^2}{m|\Delta_c|}[\frac{29}{300} + \frac{127\Gamma^2/2}{75(\Delta_c)^2+75\Gamma^2/4}]$.[17] Con-

versely, the RIR width broadens with an increase in the power of the cooling laser due to power broadening, the RIR width of which increases roughly linearly with the cooling laser power. The RIR shape is approximately the first derivative of the Gaussian velocity distribution of the cold atoms, and we can obtain the atomic temperature from the result of the RIR width.

A widely applied technique for detecting the temperature of cold atoms is the TOF method. For cold atoms in the integrating sphere, the absorption profile of a weak probe laser during TOF expansion is utilized to measure temperature and its time evolution. The resonant frequency of the probe laser has a power of 1 μW. The cooling and repumping lasers are switched on/off using the acousto-optic modulator. The TOF absorption varies with change in the power and detuning of the cooling laser, as shown in Figs. 3(a) and 3(b). The Gaussian radius σ_v of the cold atomic velocity distribution can be obtained by Gaussian fitting of the TOF signal.[32] The typical temperature T of the cold atoms is then calculated using the equation $\frac{1}{2}m\sigma_v^2 = \frac{1}{2}k_B T$, where k_B is the Boltzmann constant.

Figures 3(c) and 3(d) compare the atomic temperature measured by the TOF method and the RIR width method under different cooling laser detuning and power conditions, respectively. The difference between the two methods is within 5 μK, which is in the allowable range and may be attributed to several factors. Firstly, the unique structure of the integrating sphere makes it challenging to accurately measure the descent distance of atoms. Unlike the TOF signal in a MOT, the detected signal in the integrating sphere is not complete. Secondly, the angle between the probe and cooling laser in the integrating sphere is affected by the diffuse light field. The simplification of the parameters in the calculation also influences the temperature results in cold atoms. Furthermore, an atomic temperature below the Doppler limit indicates the properties of sub-Doppler cooling.

Due to the characteristics of the RIR signal, the spacing between the maximum of the amplification part and the minimum of the attenuation part is solely related to the detuning of the cooling laser. The probe laser detuning corresponding to the RIR peak, Δ_R, varies exclusively with the cooling laser detuning but remains invariant with changes in the power of the cooling laser. In contrast, the detuning of the probe laser corresponding to the EIA peak, Δ_E, is influenced by the relative light shift between the ground state Zeeman sublevels of the cold atoms. This relative light shift is directly proportional to the power of the cooling laser. Thus, the frequency position between the two absorption peaks (RIR peak and EIA peak) $|\Delta_R - \Delta_E|$ increases with the cooling laser power, as shown in Fig. 4(a). However, as the cooling laser detuning increases, the slopes of the RIR and EIA peak changes are 1.00342 and 1.00733, respectively. Since these slope values are nearly identical, $|\Delta_R - \Delta_E|$ remains relatively constant with changes in the cooling laser detuning, as shown in Fig. 4(e).

The cooling laser entering the integrating sphere through the multimode fiber does not undergo diffuse reflection before it touches the inner surface of the integrating sphere, and it forms four extended lasers perpendicular to the direction of the probe laser. Although these extended lasers do not slow down atoms, they contribute to the generation of EIA signals. Due to the intensity of these four extended lasers being stronger than that of the diffusely reflected laser, the laser intensity forming the EIA signal is much greater than that forming RIR, resulting in the linewidth of EIA ($\Delta\nu_E$) being much wider than that of RIR ($\Delta\nu_R$). The process of forming EIA and RIR reflects the formation of the diffuse light field, so the relationship between their absorption linewidths is closely related to the atomic cooling effect. We explore the cooling mechanism in the integrating sphere by examining the ratio $\Delta\nu_E/\Delta\nu_R$ of the EIA absorption linewidth to the RIR absorption linewidth. Experimental data reveal that when $\Delta\nu_E/\Delta\nu_R$ is approximately 1.57, the optimal detuning condition for the cooling laser is −19 MHz, and the optimal cooling laser power is 320 mW. Under these conditions, the temperature of the cold atoms reaches a minimum of 33 μK and the atom number is maximized at 9.8×10^9.

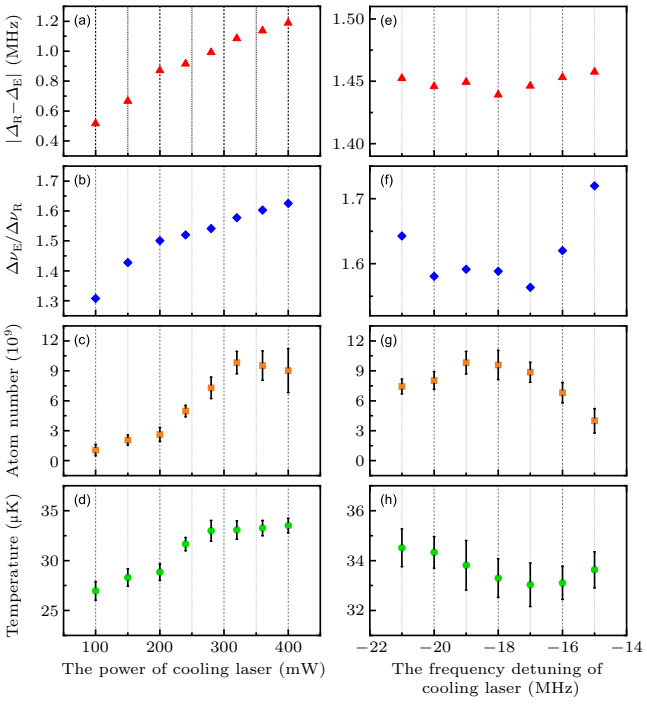


Fig. 4. (a)–(d) Dependence of $|\Delta_R - \Delta_E|$ (red triangles), $\Delta\nu_E/\Delta\nu_R$ (blue rhomboids), atom number (orange squares) and atom temperature (green circles) on the cooling laser power. (e)–(h) The variation of $|\Delta_R - \Delta_E|$ (red triangles), $\Delta\nu_E/\Delta\nu_R$ (blue rhomboids), atom number (orange squares) and temperature (green circles) with the cooling laser detunings. When $\Delta\nu_E/\Delta\nu_R$ is approximately 1.57, the detuning and power conditions for the cooling laser are −19 MHz and 320 mW. Under these conditions, the number of atoms and temperature are optimal, at 9.8×10^9 and 33 μK, respectively.

5. Conclusion

In conclusion, we have measured the nonlinear spectra of RIR and EIA in diffuse laser cooled atoms and analyzed the dependences of width and light shift on cooling laser power and detuning. The light shift of the RIR signal depends on the velocity distribution of the cold atoms, while the relative light shift between the ground state Zeeman sublevels of the cold atoms determines the light shift of the EIA signal. Consequently, the absolute difference in light shifts, $|\Delta_R - \Delta_E|$, increases with the power of the cooling laser and remains relatively constant with changes in the detuning of the cooling laser. The absorption linewidths of the RIR and EIA signals rely on the cooling laser power and detuning. When the linewidth radio $\Delta\nu_E/\Delta\nu_R$ is approximately 1.57 and the cooling laser power and detuning are 320 mW and -19 MHz, respectively, the atomic temperature is minimized at 33 μK and the number of atoms is maximized at 9.8×10^9. Therefore, the observed nonlinear spectra of RIR and EIA within the integrating spheres present a quantitative method for evaluating the cooling efficacy of these systems. This method will be applied to a cold atom magnetometer in the future, as well as other quantum sensing including cold atom clocks and cold atom interferometers.

Acknowledgments

Project supported by Shandong Provincial Natural Science Foundation (Grant No. ZR2023LLZ003), the National Natural Science Foundation of China (Grant No. 62005145), Fundamental Research Fund of Shandong University, and Shandong Provincial Postdoctoral Science Foundation (Grant No. SDBX202302002).

References

[1] Fregosi A, Gabbanini C, Gozzini S, Lenci L, Marinelli C and Fioretti A 2020 *Appl. Phys. Lett.* **117** 144102
[2] Bevilacqua G, Biancalana V, Dancheva Y and Vigilante A 2019 *Appl. Phys. Lett.* **115** 174102
[3] Maddox B and Renzoni F 2023 *Appl. Phys. Lett.* **122** 144001
[4] Cohen Y, Jadeja K, Sula S, Venturelli M, Deans C, Marmugi L and Renzoni F 2019 *Appl. Phys. Lett.* **114** 073505
[5] Behbood N, Martin Ciurana F, Colangelo G, Napolitano M, Mitchell M W and Sewell R J 2013 *Appl. Phys. Lett.* **102** 173504
[6] Taylor H A, Bounds C C, Tritt A and Turner L 2024 *Phys. Rev. Appl.* **22** 024047
[7] Aigner S, Pietra L D, Japha Y, Entin-Wohlman O, David T, Salem R, Folman R and Schmiedmayer J 2008 *Science* **319** 1226
[8] Martinez G D, Li C, Staron A, Kitching J, Raman C and McGehee W R 2023 *Nat. Commun.* **14** 3501
[9] Mcgilligan J P, Moore K R, Dellis A, Martinez G, de Clercq E, Griffin P, Arnold A, Riis E, Boudot R and Kitching J 2020 *Appl. Phys. Lett.* **117** 054001
[10] Bhardwaj K, Sarkar S, Ram S, Tiwari V and Mishra S 2023 *AIP Adv.* **13** 015108
[11] Zhang Q, Wang Y, Zhu C, Wang Y, Zhang X, Gao K and Zhang W 2020 *Chin. Phys. B* **29** 093203
[12] Tan Z, Lu B, Han C and Lee C 2024 *Chin. Phys. B* **33** 093701
[13] Zhang Y, Liu Q X, Sun J F, Xu Z and Wang Y Z 2022 *Chin. Phys. B* **31** 073701
[14] Budker D and Romalis M 2007 *Nat. Phys.* **3** 227
[15] Cheng R J, Li X X, Wang Q, Liu D J, Huang Z M, Lv S Y, Zhou Y Z, Zhang S T, Li X M and Chen Z J 2024 *Chin. Phys. B* **33** 015206
[16] Michaud F, Gattobigio G L, Tabosa J W and Kaiser R 2007 *JOSA B* **24** A40
[17] Zhao Y T, Su D Q, Ji Z H, Zhang H S, Xiao L T and Jia S T 2015 *Chin. Phys. B* **24** 093701
[18] Ji Z, Zhang H, Su D, Zhao Y, Xiao L and Jia S 2018 *J. Phys. Soc. Jpn.* **87** 024301
[19] Li J F, Wang Y F, Huang P S, Su K Y, Peng Y Q, Zhang S, Yan H and Zhu S L 2023 *Phys. Rev. Appl.* **20** 014027
[20] Fleischhauer M, Imamoglu A and Marangos J P 2005 *Rev. Mod. Phys.* **77** 633
[21] Lezama A, Barreiro S and Akulshin A 1999 *Phys. Rev. A* **59** 4732
[22] Ding D S, Zhou Z Y, Shi B S, Zou X B and Guo G C 2012 *Chin. Phys. Lett.* **29** 024202
[23] Brzozowski T M, Brzozowska M, Zachorowski J, Zawada M and Gawlik W 2005 *Phys. Rev. A* **71** 013401
[24] Grynberg G and Robilliard C 2001 *Phys. Rep.* **355** 335
[25] Sun J, Zhao P, Hu Z, Jin S, Liao R, Liu X J and Chen X 2023 *Chin. Phys. Lett.* **40** 083701
[26] Zhang W Z, Cheng H D, Liu L and Wang Y Z 2009 *Phys. Rev. A* **79** 053804
[27] Wang W, Deng J and Wang Y 2015 *J. Opt. Soc. Am. B* **32** 2441
[28] Wang W L, Dong R C, Deng J L and Wang Y Z 2016 *Phys. Rev. A* **93** 052503
[29] Guo J, Berman P, Dubetsky B and Grynberg G 1992 *Phys. Rev. A* **46** 1426
[30] Akulshin A, Barreiro S and Lezama A 1998 *Phys. Rev. A* **57** 2996
[31] Di Domenico G, Mileti G and Thomann P 2001 *Phys. Rev. A* **64** 043408
[32] Cheng H D, Zhang W Z, Ma H Y, Liu L and Wang Y Z 2009 *Phys. Rev. A* **79** 023407